Radboud University Nijmegen

Faculty of Science,
Department of High Energy Physics

Predicting event rates of long-lived, hidden particles in ATLAS and FASER

Thesis BSc Physics and Astronomy

Author:
Daniël Kooyman

Supervisor:
dr. Susanne Westhoff

Second reader:
dr. Harm Schoorlemmer

April 2025

Abstract

At the LHC, the ATLAS and FASER detectors provide opportunities for conducting dark matter searches. This study explores the possibility of coupling these two detectors by performing an analytical estimate to predict the expected event rates of long-lived particles in both. Focusing on a Higgs portal model, this work examines dark photons with masses in the range 10^{-3} to 0.5 GeV and dark scalar masses around 1 GeV. The results indicate that the optimal kinetic mixing parameter range is $[10^{-6}, 10^{-5}]$, yielding the highest combined detection probability. Nevertheless, the overall detection probabilities remain low, and the proposed coupling is expected to provide only limited additional insight.

Acknowledgements

These past few months of hard work and dedication would not have been possible without the support and encouragement of many people. I would like to express my gratitude to everyone who helped me throughout the process of completing this research and thesis.

First and foremost, I would like to thank my supervisor Susanne Westhoff for her invaluable guidance and support. Your deep knowledge and critical insights challenged me to improve, but most importantly, your enthusiasm for particle physics and your positive attitude have allowed me to pursue this internship with great passion and inspiration.

I would also like to thank Lotta van Broekhoven and Lydia Brenner for their openness and willingness to share their research with me. Your approachability and support were deeply appreciated.

Last but not least, I would like to thank my family and friends for coming to my presentation and listening to me talk about my research over and over again. Your interest and support gave me great motivation to continue and finish this thesis.

Contents

1 Introduction

Ever since the discovery of the Higgs boson at CERN, scientists have been eager to prove new theories about its properties and interactions. The Higgs boson is undeniably an intriguing particle. In some models for instance, the Standard Model (SM) Higgs boson can serve as a portal for dark matter (DM) production [1].

Dark matter is a phenomenon that obtained strong observational evidence in 1933 by Fritz Zwicky when he applied the virial theorem to galaxy clusters. He concluded that the visible mass was far too small compared to its observed gravitation [2]. This later became a widely accepted theory, with dark matter notably accounting for the observed galaxy rotation curves and velocity dispersions. The current estimate of dark matter in the universe is 85% of the total mass. Understandably, searching for evidence of dark matter has become a major focus in modern physics.

The Large Hadron Collider (LHC) at CERN in Geneva, Switzerland is a particle accelerator where they also do dark matter searches. Located on the arc of the LHC is A Toroidal LHC ApparatuS (ATLAS), a general-purpose detector optimized for detecting a wide range of particles [3]. Beams of particles, often protons, are accelerated at the LHC and collide at the interaction point (IP) of ATLAS. The newly produced and scattered particles can be identified by measuring their trajectories, energy, and momentum. However, because ATLAS is part of the LHC, it has holes along the beamline in order to let the proton beams through. Therefore ATLAS has reduced sensitivity to particles with a low transverse momentum p_T traveling close to the beamline. The ForwArd Search ExpeRiment (FASER) is more suitable for these types of particles. This significantly smaller detector is located at a 480 meter distance downstream of ATLAS IP. FASER is optimized for detecting the decay products of light and weakly interacting particles [4].

This research aims to perform an analytical estimate to predict the expected event rates of dark sector particles in ATLAS and FASER. One method of connecting the SM with a dark sector is through the use of the Higgs portal. Through this portal, SM particles are able to decay into DM particles. This separate sector called the 'dark sector' extends the *Standard Model of particle physics*. In the specific Higgs portal model used for this research, the SM Higgs boson can mix with a scalar field in the dark sector. The corresponding physical particle, known as the 'dark scalar', is denoted by S. Through this mixing, S inherits its coupling strength to SM particles from the Higgs boson. These short-lived, hidden particles S decay almost immediately into long-lived, hidden particles. The resulting particles are U(1)' gauge bosons, known as 'dark photons', denoted by Z_D. As force carriers of the dark sector, they interact weakly with SM particles via kinetic mixing with the SM photon [5]. Dark photons are particularly interesting to reconstruct due to their relatively long lifetimes, allowing them to travel far enough to reach FASER. Their decays offer insight into the properties of the dark sector and their interactions with SM particles. This provides more information on the potential constraints on Higgs portal models within ATLAS's and FASER's experimental setup.

The main goal of this study is to explore the potential coupling of ATLAS and FASER. This includes enabling the tracking of sister particles that originate from decay in ATLAS which are scattered and detected in both ATLAS and FASER. The objective is to examine if this coupling is able to obtain additional information on a model with long-lived particles (LLPs). This involves analyzing the production of dark scalars and dark photons, their lifetimes, and their decay products. This Higgs portal model was chosen for its predictions of LLP pairs at reasonably high event rates, making it a suitable model for studying the ATLAS and FASER coupling.

The organization of this thesis is as follows. The dark sector model used for this

research is described in Section 2. The expected signals and decay simulations are shown in Section 3, as well as the detector geometry and parametrization used for the detection probability. The analyzed signal results are presented in Section 4. These results are concluded and discussed in Section 5.

2 The Dark Sector

The *Standard Model of particle physics* consists of 25 elementary particles (without counting the quark colors separately), all of which play a part in one or more fundamental forces. A well-known deficiency, however, is its inability to account for dark matter and dark energy. Despite this, the Standard Model is a well-tested theory with no current accepted experiments contradicting its foundation. Therefore, a branch had been added to the theoretical models for fundamental physics labeled *Beyond the Standard Model of particle physics* (BSM). This extension of the Standard Model addresses its many shortcomings. One particular extension is called the 'Dark Sector' or Hidden Sector, a sector containing hidden particles including potential dark matter candidates. These particles have remained unmeasurable by direct detection methods to date, however colliders can potentially detect them. This section describes the Dark Sector model used for this research, along with the production and properties of its dark particles.

2.1 The Model

In order to extend the SM to contain a dark sector, a Higgs portal model is used. This Higgs portal is mediated by the SM Higgs Boson, which was first detected by the ATLAS detector in 2012 [6]. This particle is theorized to be responsible for giving mass to SM particles by electroweak symmetry breaking, also referred to as the 'Higgs Mechanism'. However, in context of the dark sector, the Higgs boson plays a crucial role in the production of dark matter candidates. If the dark sector contains a scalar field, it is possible for mixing between this scalar field and the Higgs particle to occur. This mixing is denoted by θ_ϕ, which signifies the mixing angle between the SM Higgs boson and the dark scalar. Through this mixing, the dark scalars 'borrow' the Higgs boson's interactions and properties.

With the Higgs portal allowing interactions with the dark sector, the Lagrangian of the scalar is given by [5]

$$\mathcal{L}_\Phi = |D_\mu H|^2 + D_\mu S D^\mu S - \mu^2|H|^2 - \frac{1}{2}\mu_S^2 S^2 - \lambda|H|^4 - \lambda_D S^4 - \alpha S^2|H|^2 - \beta|H|^2 S, \quad (1)$$

where the first two terms are the kinetic terms of the SM Higgs doublet H and dark scalar S, and the remaining terms denote the scalar potential. The last two terms describe the mixing between the SM Higgs and the dark scalar.

In many dark sector models as well as this one, the dark scalar has a possibility of interacting with other hidden particles. Due to the term $D_\mu S D^\mu S$, dark scalars can decay into dark photons if kinematically allowed. This is because the dark scalar is charged under the $U(1)'$ symmetry.

The dark photon field is contained in the covariant derivative $D_\mu = \partial_\mu + i g_D Z_{D\mu}$ and mixes with the hypercharge field B. The Lagrangian for dark photons is given by [7]

$$\mathcal{L}_{gauge} = -\frac{1}{4}\tilde{B}_{\mu\nu}\tilde{B}^{\mu\nu} - \frac{1}{4}\tilde{Z}_{D\mu\nu}\tilde{Z}_D^{\mu\nu} + \frac{1}{2}\frac{\epsilon}{\cos\theta_W}\tilde{B}_{\mu\nu}\tilde{Z}_D^{\mu\nu}, \quad (2)$$

where the fields with a tilde are prior to diagonalization. The last term shows the kinetic mixing of the hypercharge field B and the dark photon Z_D, denoted by ϵ. This

mixing parameter allows for the dark photon to inherit the SM photon's interactions and properties. After diagonalization, the B field mixes with the Z^0 field, resulting in the SM photon and the Z-boson. These Lagrangians will become important in Sect 2.3 where the corresponding decay widths are deduced.

2.2 Dark Scalar Production from B-meson Decay

For the aims of this work, the focus is placed on B-meson decay into dark sector particles. B-mesons are created in the high-energy proton-proton beam collisions at the LHC. A $b\bar{b}$ pair is produced as shown in the Feynman diagram in Fig. 1. B-mesons consists of a b-antiquark and a lighter quark (either u, c, d or s). The t-quark/antiquark is not expected to form a B-meson with a b-antiquark/quark due to its short lifetime. The B^--meson is formed when the b-quark interacts with a lighter antiquark ($\bar{u}$, $\bar{c}$, $\bar{d}$ or $\bar{s}$).

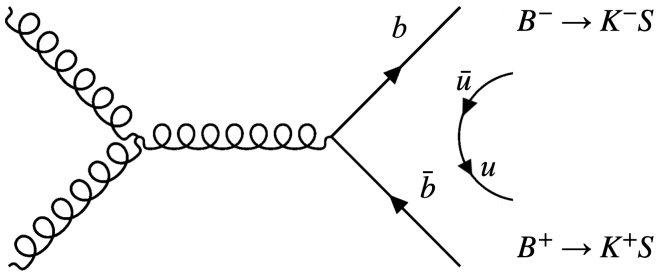

Figure 1: The production of a B-meson through a three-gluon vertex. The process results in a $b\bar{b}$ pair. One of these particles (either the bottom quark or antiquark) forms a B-meson by combining with an up antiquark or quark, respectively. This B-meson later decays into a kaon (K) and a dark scalar.

The B-meson can decay into a kaon, denoted by K, and a dark scalar S. This happens through flavor-changing neutral currents, which arise from weak interactions where b-quarks transition into s-quarks. These processes involve virtual particles forming a loop. Loop-induced processes are suppressed and therefore more rare to occur compared to tree level processes. The strength of the coupling between the b-quark and the virtual quark (u, c or t) depends on the Cabibbo–Kobayashi–Maskawa (CKM) matrix, where the top-bottom coupling has the highest value. This specific transition happens through a t, W-loop, as shown in Fig. 2.

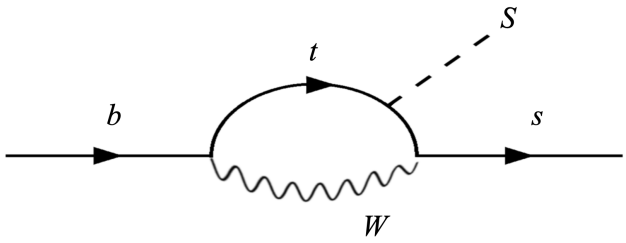

Figure 2: The t, W-loop of B-meson decays to dark scalars. The bottom quark of the B-meson decays into a dark scalar and strange quark through this loop-induced process. The top quark and W-boson are virtual particles.

Direct production $u\bar{u} \to S$ is heavily suppressed due to a weak Yukawa coupling. This coupling is the interaction between a scalar field and a fermionic field. Heavier fermions lead to a stronger Yukawa coupling, which signifies a stronger interaction with the Higgs field, resulting in a stronger $S - f - \bar{f}$ coupling strength. Due to the top quark being the heaviest quark, t, W-loops are the preferred production method of dark scalars.

2.3 Dark Particle Decays

The Lagrangians for the dark scalar S (Eq. (1)) and the dark photon Z_D (Eq. (2)) can result in the following interaction terms with the corresponding decays:

- $S \to f\bar{f}$:
$$\mathcal{L} \supset -\frac{y_f}{\sqrt{2}} \sin\theta_\phi f \bar{f} \hat{s}, \tag{3}$$
- $S \to Z_D Z_D$:
$$\mathcal{L} \supset (D_\mu S)(D^\mu S), \tag{4}$$
- $Z_D \to f\bar{f}$:
$$\mathcal{L} \supset g_L Z_{D_\mu} \bar{f}_L \gamma^\mu f_L + g_R Z_{D_\mu} \bar{f}_R \gamma^\mu f_R. \tag{5}$$

These terms induce the decays of the dark scalars and dark photons. Note that the $\hat{s}$ represents the mass eigenstate after mixing with the Higgs. Starting with the dark scalar, this particle is short-lived if it has a sizable coupling g_D to dark photons. Its short lifetime is due to the efficiency of $S \to Z_D Z_D$ decay. The mixing θ_ϕ, if large enough, allows for the decay of dark scalars back into SM fermions. The interaction in Eq. (3) then gives rise to the following decay width [5]:

$$\Gamma(S \to f\bar{f}) = \frac{1}{16\pi} m_S y_f^2 N_C \sin^2\theta_\phi \left(1 - \frac{4m_f^2}{m_S^2}\right)^{3/2}, \tag{6}$$

where m_S is the dark scalar mass, m_f is the fermion mass and y_f is the Yukawa coupling between the fermion and the Higgs field, N_C is the number of color charges (3 for quarks, 1 for leptons), and θ_ϕ is the mixing angle between the Higgs and the dark scalar. The $\hat{s}$ has been neglected. In what follows, S denotes the mass eigenstate after mixing. The likelihood of the dark scalar decaying in this channel is proportional to the coupling strength $y_f \sin(\theta_\phi)$ (see Fig. 3).

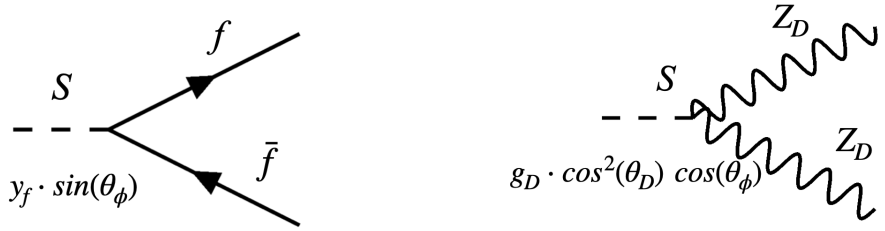

Figure 3: Feynman diagrams of dark scalar decay into SM particles (left) and dark photons (right). The corresponding coupling strengths between the incoming and outgoing particles are shown at the vertex. **Left:** Dark scalar decay into a fermion-antifermion pair. The coupling strength is denoted by $y_f \sin\theta_\phi$. **Right:** Dark scalar decay into a dark photon pair. The coupling strength is denoted by $g_D \cos{\theta_D}^2 \cos\theta_\phi$.

When looking at dark scalar decay into dark photons, the decay width is based on the Lagrangian term in Eq. (4) and is given by [8]

$$\Gamma(S \to Z_D Z_D) = \frac{1}{32\pi} g_D^2 \frac{m_{Z_D}^2}{m_S} \cos^4\theta_D \cos^2\theta_\phi \left(1 - \frac{4m_{Z_D}^2}{m_S^2}\right)^{1/2} \left(3 + \frac{m_S^4}{4m_{Z_D}^4} - \frac{m_S^2}{m_{Z_D}^2}\right), \tag{7}$$

where g_D is the coupling of the dark scalar to a dark photon pair, m_{Z_D} is the dark photon mass, and θ_D is the mixing angle between the dark photon and the hypercharge B field. The coupling strength of this decay channel is given by $g_D \cos^2\theta_D \cos\theta_\phi$ (see Fig. 3).

Dark photons are LLPs if the kinetic mixing is small. Specifically, they are able to live long enough to reach FASER before decaying. They decay exclusively into SM fermions. This study only focuses on electrons and muons for simplicity, but also because leptons are expected to be well reconstructed in both detectors. The corresponding decay width, based on Eq. (5), is given by [7]

$$\Gamma(Z_D \to f\bar{f}) = N_C Q^2 \frac{e^2\epsilon^2}{12\pi} m_{Z_D} \left(1 + \frac{2m_f^2}{m_{Z_D}^2}\right) \left(1 - \frac{4m_f^2}{m_{Z_D}^2}\right)^{1/2}, \tag{8}$$

where ϵ is the kinetic mixing parameter, Q is the electric charge of the fermion in units of e and e is the proton charge. The coupling strength of dark photon decay into SM fermions is given by ϵe (see Fig. 4).

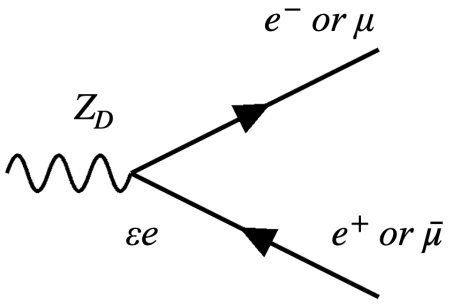

Figure 4: Feynman diagram of dark photon decay into electrons and muons. The coupling strength between dark photons and SM fermions is given by ϵe.

3 Long-lived Particle Searches at the LHC

The longevity of dark photons has proven to be an interesting aspect of dark particle searches at the LHC. This characteristic allows for a produced Z_D pair to decay into separate detectors - one in ATLAS and one in FASER. Naturally, due to the nature of dark particles, dark scalars and dark photons can not be directly detected. In order to reconstruct dark photons, detectors focus on their detectable decays into the Standard Model. This research focuses on $Z_D \to e^+e^-$ and $Z_D \to \mu^+\mu^-$ decay. This section discusses the branching ratios, decay lengths and the decay probability of dark scalars and dark photons.

3.1 Expected Signals in ATLAS and FASER

ATLAS and FASER are optimized for detecting different types of particles. ATLAS is optimized to detect particles with a relatively high transverse momentum p_T, whereas FASER detects particles that travel undisturbed along the beam line originating from the ATLAS IP. In order to maximize the decay of the sister Z_D pair in ATLAS and FASER, the particles would need to be produced at different momenta.

The pseudorapidity ranges of ATLAS and FASER also differ significantly. The pseudorapidity η describes the inclination between the beam axis and the particle's flight way, and is defined as a function of the polar angle θ, given by

$$\eta = -\ln\left[\tan\frac{\theta}{2}\right]. \tag{9}$$

In high-energy physics, the use of pseudorapidity over polar angle is often preferred because pseudorapidity differences remain invariant under Lorentz transformations of boosts along the beam axis. FASER, located at 480 meters distance from ATLAS IP, has an angular acceptance of $\eta > 9.2$ [9]. This makes it a forward detector and therefore specialized for detecting forward-traveling particles. However, due to its low angular coverage, its decay detection probability is relatively low. In contrast, ATLAS has a broader pseudorapidity range, covering both forward and backward regions. Its decay detection probability is therefore estimated to be much higher than FASER's. The detector geometries will be further elaborated on in Section 3.3.

The signal of the dark sector is described by the decay chain below:

$$\textit{B-meson} \to S \to Z_D \to \textit{SM particles},$$

where the focus is put on reconstructing a displaced Z_D pair through electron or muon pair detection.

3.2 Analyzing Decay Properties

Dark scalars are produced at ATLAS IP. For $m_S > 2m_{Z_D}$, the dark scalar is able to produce a Z_D pair through the decay width given in Eq. (7). The coupling g_D in this model is a free parameter. While perturbation theory restricts it to approximately $g_D < 1$, this study assumes $g_D = 1$ to ensure that all dark scalars decay exclusively into dark photons, rather than SM particles. For $m_S > 2m_f$, it's kinematically possible for the dark scalar to produce a fermion-antifermion pair. The Yukawa coupling, as mentioned in Eq. (6), can be written as $y_f = \sqrt{2}m_f/v$, where m_f is the corresponding SM fermion mass and $v = 246$ GeV is the vacuum expectation value (VEV). The variables m_{Z_D}, m_S, θ_D and θ_ϕ are treated as free parameters throughout this study. Appropriate values for these parameters need to be chosen in order to maintain a branching ratio of $S \to Z_D Z_D$ close to 1. The branching ratio is given by:

Fermion	Mass m_f (MeV)
e	$0.511 \pm 0.00...$
μ	$105.658 \pm 0.00...$
τ	1776.93 ± 0.09
u	2.16 ± 0.07
d	4.70 ± 0.07
s	93.5 ± 0.8
c	1273.0 ± 4.6
b	4183 ± 7
t	172570 ± 290

Table 1: SM fermion mass values taken from Ref. [10].

$$BR(S \to Z_D Z_D) = \frac{\Gamma(S \to Z_D Z_D)}{\Gamma_{tot}}, \tag{10}$$

where the total decay width, Γ_{tot}, is given by:

$$\Gamma_{tot} = \Gamma(S \to Z_D Z_D) + \sum_f \Gamma(S \to f\bar{f}), \tag{11}$$

where $f = e, \mu, u, d, s$, representing all kinematically allowed fermion-antifermion pairs for $m_S = 1.0$ GeV. The masses m_f of the SM fermions used in this study are listed in Table 1.

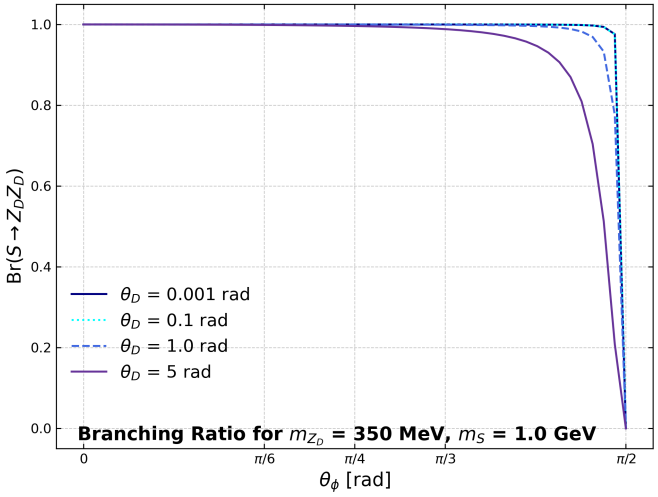

Figure 5: Branching ratios of $S \to Z_D Z_D$ as a function of the mixing angle θ_ϕ. Results are given for $m_{Z_D} = 350$ MeV, $m_S = 1.0$ GeV and various mixing angles θ_D.

The resulting branching ratios are shown in Fig. 5. Note that the only available fermion decay channels are e^+e^- and $\mu^+\mu^-$ based on the threshold condition $m_S > 2m_f$ and the neglecting of hadronic decay channels. The branching ratio scales as

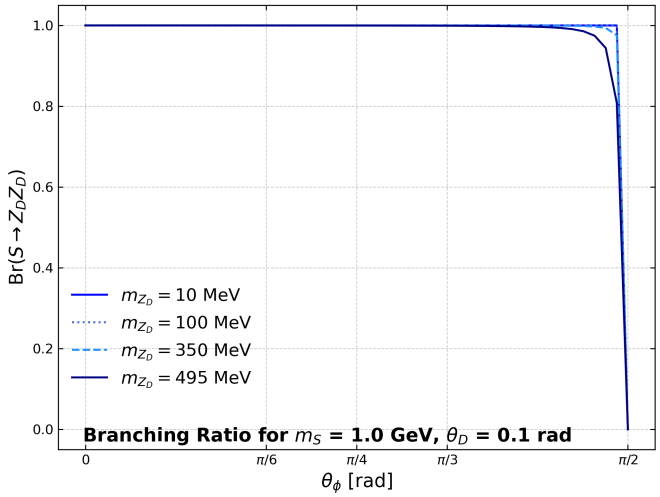

Figure 6: Branching ratio of $S \to Z_D Z_D$ as a function of θ_ϕ. Results are given for $m_S = 1.0$ GeV, $\theta_D = 0.1$ radians and various masses m_{Z_D}.

$$BR(S \to Z_D Z_D) \propto \frac{\cos^4\theta_D \cos^2\theta_\phi}{A\sin^2\theta_\phi + B\cos^4\theta_D \cos^2\theta_\phi}. \tag{12}$$

When the mixing angle $\theta_\phi \ll 1$, which is the case due to experimental bounds on θ_ϕ, Taylor expansions can be applied and the branching ratio simplifies to

$$BR(S \to Z_D Z_D) \propto \frac{\cos^4\theta_D}{\theta_\phi^2 + \cos^4\theta_D} \approx \frac{\cos^4\theta_D}{\cos^4\theta_D} = 1, \tag{13}$$

as can be seen in Fig. 5 for small angles θ_ϕ. Here, decay into the SM sector is suppressed and decay into dark photons dominates.

When looking at a larger θ_ϕ close to $\pi/2$, the branching ratio quickly drops to zero. This drop happens faster for $\theta_D \gg 1$ which leads to $\cos^4\theta_D \ll 1$, where the branching ratio simplifies to

$$BR(S \to Z_D Z_D) \propto \frac{\cos^4\theta_D \cos^2\theta_\phi / A\sin^2\theta_\phi}{1 + \cos^4\theta_D \cos^2\theta_\phi / A\sin^2\theta_\phi} \approx \frac{\cos^4\theta_D \cos^2\theta_\phi}{A\sin^2\theta_\phi}. \tag{14}$$

This shows the suppression of the dark photon decay channel under a large mixing angle θ_D. Taking a value of $\theta_D = 0.1$ radians will ensure the branching ratio will remain 1 for $m_{Z_D} = 350$ MeV and $m_S = 1.0$ GeV. A dark scalar mass of 1.0 GeV has shown to be useful as it is not too light nor too heavy. If the mass were too low, the phase space could be too limited for dark photon decay. On the contrary, if it were too high, the Z_D decay channel might become suppressed (depending on θ_D and θ_ϕ) due to other decay channels opening up.

To further investigate the behavior of the branching ratio, nearby values of m_{Z_D} have also been explored in Fig. 6. At $m_S = 1.0$ GeV, decay is not kinematically possible for $m_{Z_D} \geq 500$ MeV , therefore masses up to 450 MeV have been plotted. For a small enough angle θ_ϕ, the branching ratio remains 1 for all plotted values m_{Z_D}. Therefore, for the remainder of this work, $m_S = 1.0$ GeV is taken and values of $m_{Z_D} \in [10^{-3}, 0.5]$ GeV are considered to ensure that $m_S > 2m_{Z_D}$. θ_ϕ must be small due to experimental

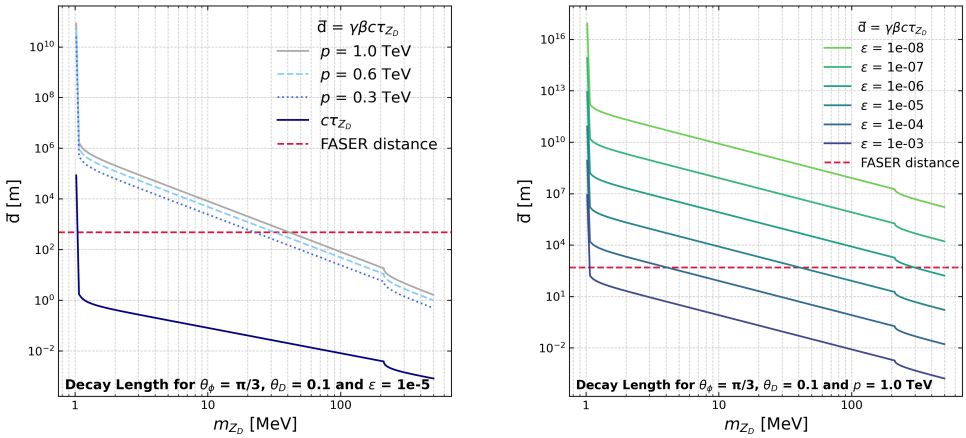

Figure 7: The decay lengths $\bar{d} = \gamma\beta c\tau_{Z_D}$ as functions of m_{Z_D}. **Left**: Results are plotted for mixing angles $\theta_\phi = \pi/3$ and $\theta_D = 0.1$ radians, kinetic mixing $\epsilon = 10^{-5}$ and various momenta p. The dark blue line represents the proper decay length. The horizontal red line represents the distance between ATLAS IP and FASER. **Right**: Results are plotted for mixing angles $\theta_\phi = \pi/3$ and $\theta_D = 0.1$ radians, momentum $p = 1.0$ TeV and various kinetic mixing parameters ϵ. Again, the horizontal red line represents the distance between ATLAS IP and FASER.

bounds.

For detection at FASER, the dark photons must travel a sufficient distance before decaying. The decay length determines the decay probability. Due to the high energies they're produced at, the particles experience significant Lorentz boosting. To account for this effect, the Lorentz-boosted decay length $\bar{d}$ in the lab frame of proton-proton collisions is defined as

$$\bar{d} = \gamma\beta c\tau, \tag{15}$$

where γ is the Lorentz-factor $1/\sqrt{1-\beta^2}$, β is the ratio v/c, v is the velocity of the particle, c is the speed of light and τ is the lifetime of the particle, in this case Z_D. The lifetime scales with the decay width as $\tau = 1/\Gamma$, assuming natural units ($\hbar = 1$ and $c = 1$). The Lorentz-boosted decay length defines the distance traveled before decay is measured in the laboratory frame. The proper decay length d can be found by removing the Lorentz-factors γ and β. This expression results in $d = c\tau_{Z_D}$ which gives the distance the particle would travel if it were moving at speed c for time τ.

For this study, it is more practical to express the dark photon's decay length in terms of momentum. Using the relationship $p = \gamma m v$, the Lorentz-boosted decay length can be rewritten as

$$\bar{d} = \frac{p}{m_{Z_D} c} c\tau_{Z_D} = \frac{p}{m_{Z_D}} \tau_{Z_D}, \tag{16}$$

where m_{Z_D} is the mass of the dark photon and p the absolute value of the dark photon 3-momentum.

Fig. 7 presents the results for the dark photon decay lengths as functions of Z_D masses. For simplicity, this work only includes e^+e^- and $\mu^+\mu^-$ decays, neglecting the

hadronic decay channels. This restricts the range of m_{Z_D} masses to $m_{Z_D} < 2m_\tau$. The decay lengths change distinctly at the $m_{Z_D} > 2m_e$ and $m_{Z_D} > 2m_\mu$ thresholds, where new decay channels open up.

Higher momentum dark photons travel significantly farther, leading to a higher decay length as seen in both figures. The plotted momenta p values in the left figure are $p = 0.3, 0.6$ and 1.0 TeV, based on plotted momentum distribution peaks [11]. For the right figure, a constant value of $p = 1.0$ TeV was chosen. As seen in the left figure, dark photons for $m_{Z_D} = 350$ MeV are unable to reach FASER (for the chosen value of ϵ), even for momenta as high as $p = 1.0$ TeV. The figure on the right shows that this is possible for smaller kinetic mixing parameters ϵ. This shows that a kinetic mixing value of at least $\epsilon > 10^{-6}$ is required in order for dark photons of mass $m_{Z_D} = 350$ MeV to reach FASER.

The branching ratio of dark photons with masses ranging from $0 - 500$ MeV are shown in Fig. 8. These ratios agree with those in Refs. [12, 13] up to the hadronic thresholds.

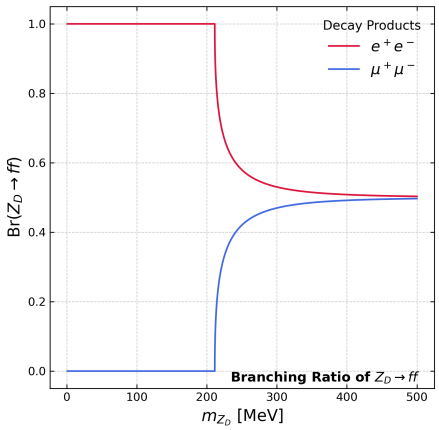

Figure 8: Branching ratios for dark photon decay into electron and muon pairs.

3.3 Dark Photon Decay Inside ATLAS and FASER

The detector geometry of ATLAS and FASER needs to be parametrized in order to approximate the amount of decays in the detectors. All following detector geometry is based on the following literature: ATLAS Refs. [14–16] and FASER Refs. [9, 17–19].

The ATLAS detector is 46 meters long and has a diameter of 25 meters. ATLAS IP, where all events occur, is positioned midpoint of ATLAS. Located at the center of ATLAS is its inner detector which consists of a pixel detector, semiconductor tracker and transition radiation tracker. The pixel detector is positioned 3.3 centimeters from the LHC beam. The active components of the pixel detector this work focuses on are the barrel layers and the end-caps. Their lengths, radii and pseudorapidity-reaches are visualized in Fig. 9. The minimum length L_{min} at which a particle needs to have traveled before decay in order to be detectable as a displaced vertex is chosen to be $200 \cdot 10^{-6}$ meters for this study [20]. The particle needs to pass at least four layers of tracking elements for detection [21].

FASER is located at 480 meters from ATLAS IP, has an aperture radius of 0.1 meters and a decay volume of 1.5 meters. FASERν is not included in this reach, this work only

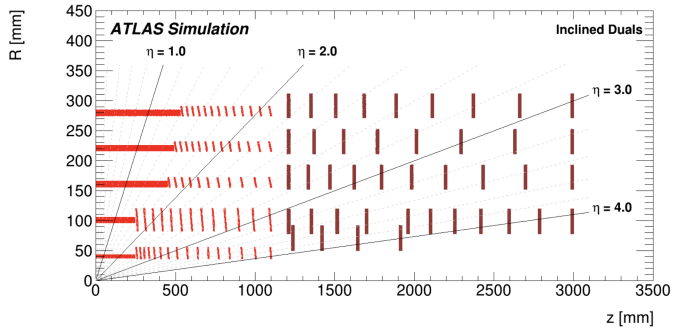

Figure 9: A look into ATLAS's Pixel Detector taken from Ref. [14]. Only a quadrant of the detector is shown. The red lines represent the barrel layers, the dark red lines represent the end-cap rings. The beamline runs along the horizontal axis where zero presents ATLAS IP. The black lines represent the pseudorapidity η.

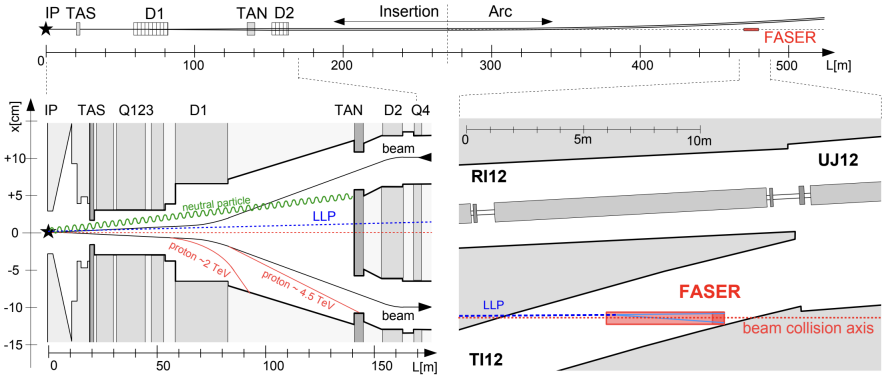

Figure 10: A schematic view of the forward region of ATLAS with various particle trajectories taken from Ref. [22]. **Top**: FASER is located at a 480 meter distance from ATLAS IP along its beam axis, represented by the dotted line. **Bottom left**: Various high-energy particle trajectories sketched from ATLAS IP. LLPs are able to pass through the structures unaffected. **Bottom right**: LLPs have the possibility of reaching FASER, passing through 90 meters of rock and 10 meters of concrete in transit.

focuses on the main detector. For detection to be possible, the minimum length for detectable decay is set to 5 meters before the main detector. The solid rocks through which these particles travel can absorb the decay products if these are produced too early. FASER's closed off build from the LHC allows it to detect particles flying within close range of the beamline. For simplification purposes, FASER's pseudorapidity range is approximated as $\eta = \infty$. Its minimum pseudorapidity is $\eta > 9.2$. For two tracks to be detectable, both particles need to pass at least two layers. However, in the case of a displaced decay, only one track will be detectable in FASER. In that case, three hits are required for detection [21]. FASER's location downstream ATLAS is visualized in Fig. 10. The intervals (L, η) per detector part from Figs. 9 and 10 are summarized in Table 2.

For dark photons produced in dark scalar decays, the probability of decay within a detector is given by [5]

$$P_{Z_D}^{det}(p_{Z_D}, \theta_{Z_D}) = (e^{-L_{\min}/\bar{d}} - e^{-L_{\max}/\bar{d}})\Theta(R - \tan\theta_{Z_D} L_{\max}), \tag{17}$$

where R is the radius of the detector and the decay length constraints (L_{min}, L_{max}) are covered by the first term and the second term ensures the angular acceptance of the detector. Since the beamline aligns with the z-axis, the detector is symmetric in z and therefore the coordinates can be reduced to (x, y), or preferably in polar coordinates (r, θ). Normalization of the integral over the full angular plane $[0, \pi]$ leads to an extra factor of $1/2$. The lengths (r_{min}, r_{max}) can be substituted for $(\frac{L_{min}}{\cos\theta_{Z_D}}, \frac{L_{max}}{\cos\theta_{Z_D}})$. This leads to the following integral:

$$\begin{aligned} P_{Z_D}^{det,int}(p_{Z_D}, \theta_{Z_D}) &= \frac{1}{2}\int_{\theta_{min}}^{\theta_{max}} \sin(\theta) d\theta \int_{r_{min}}^{r_{max}} \frac{1}{\bar{d}} e^{-r/\bar{d}} dr \\ &= \frac{1}{2}\int_{\theta_{min}}^{\theta_{max}} \sin(\theta) \left(e^{-L_{min}/\bar{d}\cos(\theta)} - e^{-L_{max}/\bar{d}\cos(\theta)} \right) d\theta. \end{aligned} \tag{18}$$

This expression represents a more general form of Eq. 17, obtained by integrating over the detector's angular acceptance. Eq. 18 fully describes the detection probability of Z_D decay within the detector volume defined by bounds (L, θ), assuming a tracker detection efficiency of 100%.

Detector Component	L_{min} (m)	L_{max} (m)	η_{min}	η_{max}
ATLAS Barrel Layers	$200 \cdot 10^{-6}$	0.450	1.6	1.8
		0.590	1.8	2.0
		0.960	2.0	2.2
		0.920	2.2	2.4
ATLAS End-caps	$200 \cdot 10^{-6}$	1.200	2.4	2.6
		1.460	2.6	2.8
		1.790	2.8	3.0
		1.970	3.0	3.2
		1.500	3.2	3.4
		1.940	3.4	3.6
		2.100	3.6	3.8
		2.400	3.8	4.0
FASER Main Detector	475	481.5	9.2	∞

Table 2: Detector (L, η) intervals for ATLAS barrel layers, end-caps, and FASER, taken from Figs. 9 and 10. L_{min} shows the minimum length at which the dark photon needs to travel before a displaced decay can be detectable. L_{max} shows the maximum length at which the decay products of the dark photon are able to pass through four tracking layers. η_{min} and η_{max} show the minimum and maximum ranges in pseudorapidity.

4 Signal Results

This section analyzes the probability of detecting Z_D decays in ATLAS and FASER. The detection probability in Eq. 18 has been plotted against various dark photon decay lengths for FASER as well as ATLAS, where its Pixel Detector components are compared. Furthermore, the efficiency of the potential coupling of ATLAS and FASER are examined.

4.1 ATLAS Pixel Detector

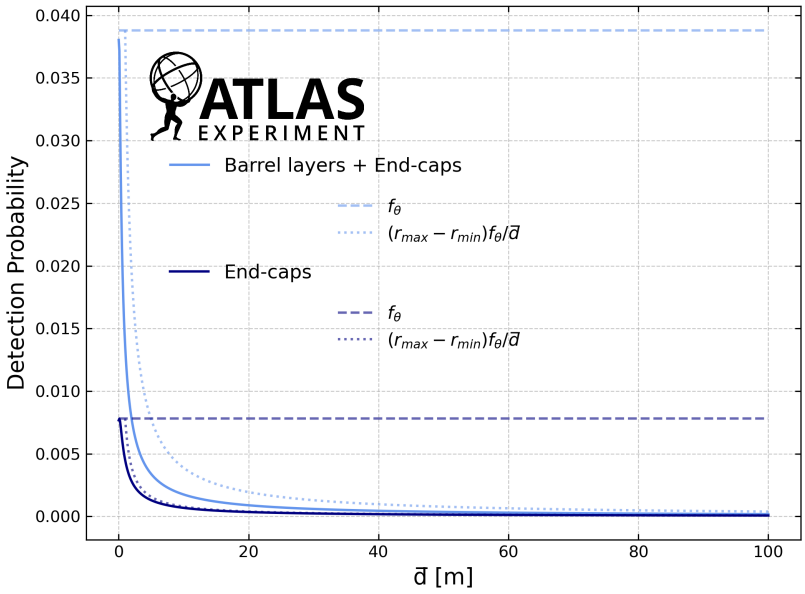

Figure 11: The detection probability $P_{Z_D}^{det}$ from Eq. (18) in ATLAS plotted against the decay length $\bar{d}_{Z_D}$ ranging from 0 to 100 meters. The dark blue line represents the end-cap rings, using the 'ATLAS End-caps' intervals from Table 2. The light blue line represents the barrel layers and end-cap rings, using both the intervals 'ATLAS End-caps' and 'ATLAS Barrel layers' from Table 2. The dashed lines f_θ represent the angular coverage of the corresponding detector components. The dotted lines $(r_{max} - r_{min})f_\theta/\bar{d}$ represent the asymptotic behavior of $P_{Z_D}^{det}$ for instances where $L_{max} \ll \bar{d}$.

Fig. 11 shows the results for Z_D decay in ATLAS. Dark photons are produced close to ATLAS IP due to the short lifetimes of dark scalars. Therefore, ATLAS can only detect dark photons with a relatively short decay length. The decay lengths $\bar{d}$ have accordingly been plotted in the range of 0 to 100 meters.

Smaller decay lengths where $L_{min} < \bar{d} < L_{max}$ illustrate a peak in the detection probability. However, the angular coverage of ATLAS significantly influences its ability to detect decays. Particles that fly too close to the beamline can escape through the aperture, rendering them undetectable. To estimate the maximum percentage of detectable particles by ATLAS, the angular coverage is calculated as a fraction of the detector's angular bounds over the entire angular plane:

$$f_\theta = \frac{\int_{\theta_{min}}^{\theta_{max}} \sin(\theta) d\theta}{\int_0^{\pi} \sin(\theta) d\theta}. \tag{19}$$

Taking ATLAS's barrel layers and end-caps interval bounds from Table 2 yields values in pseudorapidity. These must first be converted to polar angles in degrees using Eq. (9) before being expressed in radians for evaluating the integral. This results in the following angular coverage fractions f_θ:

$$f_{\theta,\ BL+EC} = \frac{\int_{0.0366}^{0.398} \sin(\theta) d\theta}{2} \approx 0.0387; \tag{20}$$

$$f_{\theta,\ EC} = \frac{\int_{0.0366}^{0.180} \sin(\theta) d\theta}{2} \approx 0.00774, \tag{21}$$

corresponding to the barrel layers plus end-caps, and end-caps only, respectively. These values are illustrated in Fig. 11, where the peaks in detection probability align well with the respective angular coverages f_θ.

For instances where the decay length $\bar{d}$ is much larger than the maximum tracking length, the detection probability naturally converges to zero. To evaluate this asymptotic behavior, let $L_{max} \ll \bar{d}$ so that $r/\bar{d} \ll 1$ (for $\cos\theta \gg 0$):

$$P_{Z_D}^{det} \propto \int \frac{1}{\bar{d}} e^{-r/\bar{d}} dr \approx \int \frac{1}{\bar{d}} dr = \frac{r_{max} - r_{min}}{\bar{d}}. \tag{22}$$

Taking the angular coverage into account, the approximation becomes $\frac{f_\theta}{\bar{d}} \cdot (r_{max} - r_{min})$, as shown in Fig. 11. For the barrel layers plus end-caps, there appears to be a significant deviation between the exact plot and the approximated plot for small $\bar{d}$. This follows evidently from the limit $L_{max} \ll \bar{d}$ not being satisfied in this region. For larger values $\bar{d}$, the approximations are conform with the exact plots. The approximation for the end-caps, however, appears to be close to the exact plot regardless of small $\bar{d}$. This is due to the smaller scattering angle θ in the end-caps, which leads to a larger $\cos\theta$, resulting in the ratio $r/\bar{d} = L_{max}/\cos\theta\bar{d} \ll 1$ and thus a more accurate first-order approximation, provided that $L_{max}^{BL} = L_{max}^{EC}$.

The barrel layers plus end-caps plot shows a higher detection probability than the end-caps only. Due to the dependency of the production rate of Z_D on θ_D, this increase of detection probability is not related to a larger areal coverage. It is therefore more probable that the barrel layers plus end-caps cover a largerθ_D range in which Z_D pairs are more likely to decay. For the analysis of the coupling of ATLAS and FASER, both the barrel layers and end-caps will be included in the defined intervals.

4.2 FASER Main Detector

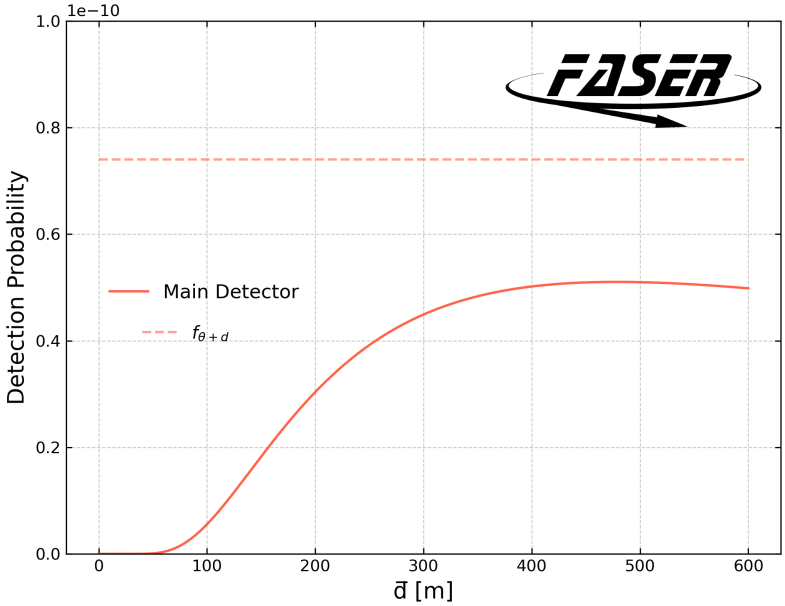

Figure 12: The detection probability $P^{det}_{Z_D}$ from Eq. 18 in FASER plotted against the decay length $\bar{d}_{Z_D}$ ranging from 0 to 600 meters. The solid line represents the main detector, using the intervals 'FASER Main Detector' from Table 2. The dashed line f_θ represents the angular coverage.

Results for Z_D decay in FASER are shown in Fig. 12. Considering FASER's distance from ATLAS IP, decay lengths $\bar{d}$ have been plotted in a suitable range of 0 to 600 meters. The decay probability of FASER is plotted with the assumption that dark photons are evenly produced over the phase space. In reality, B-mesons are produced at a relatively small inclination relative to the beam line. As a result, FASER's detection probability may differ in practice.

Looking at the region where $\bar{d} \ll L_{min}$, the detection probability collapses to zero. This is to be expected since these particles decay long before reaching the minimum tracking length required by FASER. The integral confirms this as the exponential function tends to zero for $\bar{d}/r \ll 1$.

To examine the spatial coverage of FASER, we take the angular coverage from Eq. 19 and add its fractional distance from ATLAS IP, defined by:

$$f_d = \frac{6.5}{2 \cdot 481.5}, \tag{23}$$

where the trackable area is $\Delta L = L_{max} - L_{min} = 6.5$ meters and $2 \cdot 481.5$ meters is the total distance from ATLAS IP to FASER in the positive and negative plane. The total spatial coverage then becomes:

$$f_{\theta+d,\ FASER} = \frac{6.5 \cdot \int_0^{0.000209} sin(\theta) d\theta}{4 \cdot 481.5} \approx 7.371 \cdot 10^{-11}. \tag{24}$$

This approximation is plotted as f_θ in Fig. 12. The line corresponds to the peak of the probability distribution, with a slight deviation of approximately $1 \cdot 10^{-11}$. As

anticipated, the peak lies within the detector range, around $\bar{d} = 480$ meters. For decay lengths $\bar{d} > L_{max}$, the probability gradually drops to zero. Despite its clear peak, FASER's probability of detecting dark photon decays remains low due to its limited angular and spatial coverage.

4.3 ATLAS and FASER Coupling

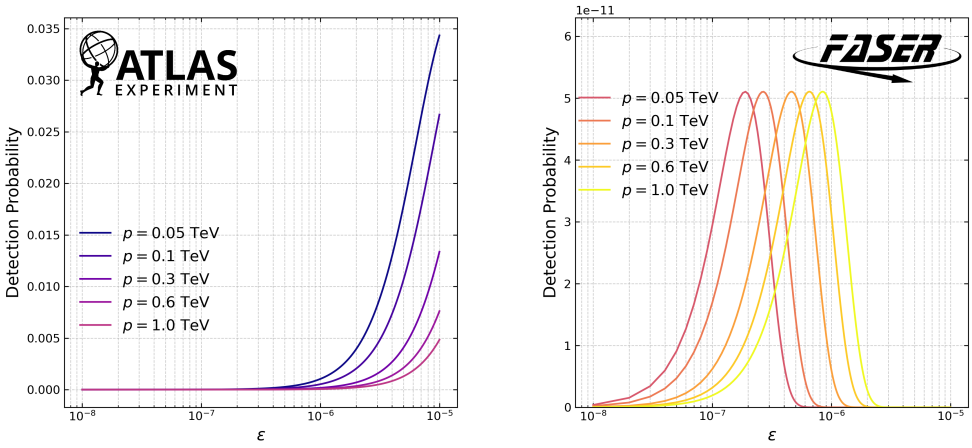

Figure 13: The detection probabilities inside ATLAS and FASER plotted as functions of kinetic mixing ϵ with various momenta p, ranging from 0.05 to 1.0 TeV. **Left**: Results are plotted for ATLAS's barrel layers and end-caps. **Right**: Results are plotted for FASER's main detector.

Fig. 13 shows the results of the detection probability as a function of the kinetic mixing ϵ for ATLAS and FASER. The specific momenta values are based on Ref. [11]. The dependence of the decay length on the kinetic mixing parameter ϵ has a significant influence on the detection probability. As noticeable in both plots, a large ϵ leads to shorter decay lengths, whereas a smaller ϵ results in longer decay lengths. This is explained by the relation $\bar{d} \propto \frac{1}{\epsilon^2}$. To display peaks for both detectors whilst keeping the range limited to values where detection is possible in each, ϵ is plotted from 10^{-8} to 10^{-5}.

The left figure represents the detection probability in ATLAS using its barrel layers plus end-cap rings. As mentioned before, lower kinetic mixing values correspond with higher decay lengths, leading to fewer detectable decays within ATLAS. The probability starts to gradually increase around $\epsilon \sim 5 \cdot 10^{-7}$. It is evident that probability peaks for ATLAS occur around higher kinetic mixing parameter values, which are not included in the plotted range.

The figure on the right displays FASER's detection probability in its main detector. Higher momenta show distributions in ranges of higher kinetic mixing values, whereas lower momenta are dominating on the lower end of the plotted ϵ range. The maximum values visually correspond to the peak in Fig. 12.

5 Discussion and Conclusion

The aim of this research was to predict event rates of dark photons in both ATLAS and FASER, exploring potential coupling constraints. Considering the results of Fig. 13, the most favorable region for decay detection of a displaced Z_D pair, one occurring in ATLAS and the other one in FASER, corresponds to kinetic mixing parameter values $\epsilon \sim 10^{-6}$ to 10^{-5}. The particles decaying in ATLAS require a low momentum, contrasting the decaying particles in FASER with high momenta.

The range 10^{-6} to 10^{-5} for ϵ is on the low end of typical ranges for searches in ATLAS, especially when compared to Refs. [23,24]. These sources researched different dark photon production methods that lead to ranges of $\epsilon \in [10^{-8}, 10^{-2}]$ and $\epsilon^2 \in [10^{-7}, 10^{-3}]$, respectively. Ref. [23] shows higher branching ratio densities for $\epsilon \in [10^{-5}, 10^{-4}]$ for similar dark photon masses. The kinetic mixing ranges for Ref. [24] are similar, but this source uses heavier dark photons compared to this study. However, this study's focus was searching for combinations of short-lived and long-lived dark photons, which results in lighter dark photon masses and a less ideal kinetic mixing region for ATLAS.

Compared to other long-lived particle searches at FASER such as Refs. [13, 25, 26], the results for the kinetic mixing range $\epsilon \sim [10^{-8}, 10^{-5}]$ seem to match. The literature cited shows sensitivity ranges of $\epsilon \in [10^{-6}, 10^{-4}]$ for light dark photon masses in the same range as this study. Particles with a higher momentum fit the kinetic mixing ranges of existing literature.

It is important to note this study relies on several assumptions and neglected factors that may alter the actual detection probability:

- A tracking efficiency of 100% is assumed, indicating that all decays within the minimum and maximum tracking lengths shall be detected. In reality, limitations such as background noise and reconstruction inefficiencies result in a lower tracking efficiency.
- Dark photons are produced with a momentum distribution. However, for simplicity purposes, this study assumes fixed momentum values without accounting for the momentum distributions. This approximation affects the detection probability.
- Dark photon production depends on the angle relative to the beam line. In this study, an even phase-space production is assumed, leading to an altered detection probability.
- Both detector geometries in this study may slightly differ from their actual measurements. ATLAS includes approximations that may be affected by human error. As for FASER, the upper pseudorapidity limit was assumed to near infinity. In reality, a small fraction of particles is able to escape through the small aperture.
- This study only focuses on the pixel detector elements of ATLAS and the main detector of FASER. These detectors contain more components, extending the spatial coverage and are therefore more likely to detect more decays.

Additionally, choosing a different model will likely lead to different results as varying decay widths result in different decay lengths. Nevertheless, for the dark photon mass range examined in this study ($m_{Z_D} \in [10^{-3}, 0.5]$ GeV), the kinetic mixing parameter values leading to a maximized detection probability are expected to remain within similar range. This is supported by previous studies, which used different models and experimental constraints but found comparable results [25, 26].

As for a potential coupling of ATLAS and FASER, the suggested range of $\epsilon \in [10^{-6}, 10^{-5}]$ yields the highest number of detections in both detectors. Although even within this optimal range, the overall detection probability remains relatively low. The

coupling of these detectors within this study's chosen dark sector model is therefore expected to provide limited extra insight. Further exploration of alternative dark sector models may reveal more promising detection opportunities.

Future work could extend this study by exploring additional decay channels of the dark scalar, such as those involving quarks or heavier leptons, which become relevant for larger dark photon and dark scalar masses. Looking into realistic angular and momentum distributions for dark photon production and decay would also improve the accuracy of the detection probability. Furthermore, it would be useful to investigate alternative production channels beyond B-meson decays that exist in abundance at the LHC.

The results of this research may also offer useful insight for future detector design, such as improving tracking layers or integrating data from both ATLAS and FASER in the context of dark photon production. By identifying the most favorable decay detection regions within the detectors, this study can help guide future efforts toward the most promising areas of dark sector parameter space.

References

[1] ATLAS Collaboration/CERN, "The Higgs boson: a landmark discovery — CERN Accelerating Science/ATLAS Experiment." https://atlas.cern/Discover/Physics/Higgs#:~:text=By%20studying%20the%20production%20and,the%20all%2Dpervasive%20Higgs%20field, 2025. [Online; accessed 9-February-2025].

[2] F. Zwicky, "Republication of: The redshift of extragalactic nebulae," *General Relativity and Gravitation*, vol. 41, pp. 207–224, Jan. 2009.

[3] CERN, "ATLAS — CERN Accelerating Science." https://home.cern/science/experiments/atlas, 2025. [Online; accessed 9-February-2025].

[4] CERN, "FASER — CERN Accelerating Science." https://www.home.cern/science/experiments/faser, 2025. [Online; accessed 9-February-2025].

[5] J. L. Feng, I. Galon, F. Kling, and S. Trojanowski, "Dark higgs bosons at the forward search experiment," *Physical Review D*, vol. 97, Mar. 2018.

[6] The ATLAS Collaboration, "Observation of a new particle in the search for the standard model higgs boson with the ATLAS detector at the LHC," *Physics Letters B*, vol. 716, p. 1–29, Sept. 2012.

[7] D. Curtin, R. Essig, S. Gori, and J. Shelton, "Illuminating dark photons with high-energy colliders," *Journal of High Energy Physics*, vol. 2015, Feb. 2015.

[8] T. Araki, K. Asai, H. Otono, T. Shimomura, and Y. Takubo, "Dark photon from light scalar boson decays at FASER," *arXiv.org*, Nov. 2022.

[9] "Search for Axion-like Particles in Photonic Final States with the FASER Detector at the LHC," tech. rep., CERN, Geneva, 2024.

[10] S. Navas *et al.*, "Review of particle physics," *Phys. Rev. D*, vol. 110, no. 3, p. 030001, 2024.

[11] L. van Broekhoven, Private Communication, Feb. 2025.

[12] P. Ilten, Y. Soreq, M. Williams, and W. Xue, "Serendipity in dark photon searches," *Journal of High Energy Physics*, vol. 2018, June 2018.

[13] A. Ariga, T. Ariga, J. Boyd, F. Cadoux, D. W. Casper, Y. Favre, J. L. Feng, D. Ferrere, I. Galon, S. Gonzalez-Sevilla, S.-C. Hsu, G. Iacobucci, E. Kajomovitz, F. Kling, S. Kuehn, L. Levinson, H. Otono, B. Petersen, O. Sato, M. Schott, A. Sfyrla, J. Smolinsky, A. M. Soffa, Y. Takubo, E. Torrence, S. Trojanowski, and G. Zhang, "FASER's physics reach for long-lived particles," *Physical Review D*, vol. 99, May 2019.

[14] "Technical Design Report for the ATLAS Inner Tracker Pixel Detector," tech. rep., CERN, Geneva, 2017.

[15] CERN, "ATLAS — CERN Accelerating Science." https://atlas.cern/Resources/Fact-sheets, 2025. [Online; accessed 26-March-2025].

[16] G. Aad *et al.*, "The ATLAS experiment at the CERN large hadron collider: a description of the detector configuration for run 3," *Journal of Instrumentation*, vol. 19, p. P05063, May 2024.

[17] F. Collaboration, A. Ariga, T. Ariga, J. Boyd, D. W. Casper, J. L. Feng, I. Galon, S.-C. Hsu, F. Kling, H. Otono, B. Petersen, O. Sato, A. M. Soffa, J. R. Swaney, and S. Trojanowski, "Letter of intent for faser: Forward search experiment at the lhc," 2018.

[18] CERN, "FASER — Detector Design." https://faser.web.cern.ch/about-the-experiment/detector-design, 2025. [Online; accessed 25-March-2025].

[19] H. Abreu *et al.*, "The FASER detector," *Journal of Instrumentation*, vol. 19, p. P05066, May 2024.

[20] L. Wolfgang and ATLAS Collaboration, "ATLAS inner tracking detectors: Run 1 performance and developments for run 2," *Nuclear and Particle Physics Proceedings*, vol. 273-275, pp. 1134–1140, 2016.

[21] L. Brenner, Private Communication, Dec. 2024.

[22] FASER Collaboration *et al.*, "Technical proposal for faser: Forward search experiment at the lhc," 2018.

[23] G. Aad *et al.*, "Search for light long-lived neutral particles that decay to collimated pairs of leptons or light hadrons in pp collisions at $\sqrt{s} = 13$ tev with the ATLAS detector," *Journal of High Energy Physics*, vol. 2023, June 2023.

[24] G. Aad *et al.*, "Search for dark photons in rare Z boson decays with the ATLAS detector," *Physical Review Letters*, vol. 131, Dec. 2023.

[25] M. Graham, C. Hearty, and M. Williams, "Searches for dark photons at accelerators," *Annual Review of Nuclear and Particle Science*, vol. 71, p. 37–58, Sept. 2021.

[26] H. Abreu *et al.*, "Search for dark photons with the FASER detector at the LHC," *Physics Letters B*, vol. 848, p. 138378, Jan. 2024.